Applied Catalysis B: Environmental 162 (2015) 483–493

Contents lists available at ScienceDirect

Applied Catalysis B: Environmental

journal homepage: www.elsevier.com/locate/apcatb

Reaction temperature controlled selective hydrogenation of dimethyl oxalate to methyl glycolate and ethylene glycol over copper-hydroxyapatite catalysts

Chao Wen[a], Yuanyuan Cui[a], Xi Chen[a], Baoning Zong[b], Wei-Lin Dai[a,*]

[a] Department of Chemistry and Shanghai Key Laboratory of Molecular Catalysis and Innovative Materials, Fudan University, Shanghai 200433, PR China
[b] State Key Laboratory of Catalytic Materials and Reaction Engineering, Research Institute of Petroleum Processing, China Petroleum & Chemical Corporation, Beijing 100083, PR China

ARTICLE INFO

Article history:
Received 26 May 2014
Received in revised form 8 July 2014
Accepted 10 July 2014
Available online 18 July 2014

Keywords:
Hydroxyapatite
Copper based catalysts
Dimethyl oxalate
Methyl glycolate
Ethylene glycol

ABSTRACT

Copper based hydroxyapatite (HAP) supported (Cu/HAP) catalysts are synthesized by a facile ammonia-assisted one-pot synthesis (AAOPS) method and carefully studied on the selective hydrogenation of dimethyl oxalate (DMO). The Cu/HAP catalysts exhibit different catalytic performance compared with the conventional Cu/SiO_2 ones. When the reaction temperatures are set at 483 K, the optimal Cu/HAP catalyst displays relatively high and stable catalytic performance with methyl glycolate (MG) as the main product. The yield to MG can reach 70% which is the highest value on the copper based catalysts till now. When the reaction temperature is risen to 513 K, the selectivity of the catalysts swifts to the ethylene glycol (EG), and the catalytic behavior is similar to the traditional Cu/SiO_2 catalysts. It was found that the copper phosphate species play important roles in stabilizing the copper particles and the Cu^+ species. Also, the abundant surface hydroxy groups on the catalysts are responsible for the distinct catalytic performance of the Cu/HAP catalysts.

1. Introduction

As the increasing emerge of the energy crisis and environmental issue, searching for the catalytic methods for the rational and clean utilization of the coal resources and further synthesis of highly value-added chemicals are greatly needed to meet the challenging environmental needs and industrialization requirements, which consequently sparked a rapid global development of the C1 chemistry. Hydrogenation of dimethyl oxalate (DMO) to ethylene glycol (EG) is one of the great productive applications for the C1 chemistry which have been scaled up to industrial levels with a capacity of 10,000 tons per year in 2010 [1]. Furthermore, partial hydrogenation of DMO could obtain methyl glycolate (MG), the latter of which is an essential intermediate for the synthesis of pharmaceutical products, fine chemicals, and perfumes [2]. More encouragingly, ethanol (EtOH), as one of the versatile feed stock for the synthesis of various products and an additive or a potential substitute for gasoline, could also be produced by deep hydrogenation of DMO with a satisfying yield of 91% [3]. The tandem hydrogenation of DMO could obtain three main products and the development of a proper and efficient catalyst to control the synthesis of the target products continues to be a huge challenge for both academia and industry. As the primary hydrogenation product, the synthesis of MG via DMO needs a moderate reaction condition and a catalyst with relatively weak hydrogenolysis property, and generally, silver based catalysts are usually adopted. For the product of EG and deep hydrogenation product of EtOH, copper based catalysts show excellent catalytic performance and now has been intensively investigated [4–7]. To the best of our knowledge, there is no copper based catalyst with bi-functional active sites that can obtain the high yields of MG and EG respectively with the only modulation of the reaction parameters. Once the reaction products of EG and MG could be selectively controlled by the modulation of the operational conditions such as H_2 pressure, temperature or mole ratio of H_2/DMO, it would be greatly economical and energy-efficient for the DMO hydrogenation process along with the market demands.

The well-established Cu/SiO_2 catalysts are extensively studied due to its high catalytic performance on the gas-phase hydrogenolysis of the DMO to EG and EtOH. Optimized Cu/SiO_2 catalysts now have obtained an inspiring achievements with the EG yield at 100% and EtOH yield at 91% [3,5]. However, the selectivity to MG on

* Corresponding author. Tel.: +86 5566 4678; fax: +86 5566 5572.
E-mail address: wldai@fudan.edu.cn (W.-L. Dai).

http://dx.doi.org/10.1016/j.apcatb.2014.07.023
0926-3373/

the copper based catalysts is extremely low because of the superb hydrogenolysis ability of the copper species and MG would be the main hydrogenation products only when the conversion of DMO is below 70% which also indicates that the catalysts are deactivated [4]. The synthesis of MG is generally based on the carboxylation of formaldehyde over concentrated sulphuric acid or boron trifluoride catalysts [8–10]. This process involves strong acid and high reaction pressure which requires expensive equipment, and also causes severe corrosion of the reactor. Hydrogenation of DMO to MG on the Ru based homogeneous catalysts was extensively studied in 1980s [11,12], and the yield of MG could achieve up to 97%. However, homogeneous noble metal catalysts are scarce, costly and difficult to be recycled thus makes the MG production gloomy. Recently, the flourishing developed coal to ethylene glycol (CTEG) program in China rekindles the research of the hydrogenation of DMO on the heterogeneous catalysts and the synthesis of MG via DMO has gained breakthroughs. Yin et al. have found that the silver based silica catalysts show high selectivity to MG at the temperature of 463 K and could prevent further reaction to EG or EtOH [2,13]. Zheng et al. developed a kind of Ag/SBA-15 catalyst with Ag crystallite size of ca. 3.9 nm. The Ag/SBA-15 catalyst showed superb selectivity to MG with a high TOF value [14]. The Au–Ag bimetallic catalyst supported on SBA-15 is also found to exhibit excellent activity for the selective hydrogenation of DMO to MG under low temperature [15]. Although the hydrogenation of DMO to MG could be obtained with a yield over 90%, the usage of gold or silver enormously increases the production cost and the high sensibility on the reaction environment for the noble metals also blocks the industrialization of the hydrogenation of DMO process. Furthermore, Ag based catalysts are greatly susceptible to the liquid hourly space velocity (LHSV), and these catalysts are active only if the reaction LHSV is below 0.6 h^{-1}. Silica supported Cu–Ag catalysts display better selectivity to MG with a yield at 60% under higher LHSV [16]. Furthermore, the silica support could be a fatal flaw in the DMO hydrogenation process because of the leaching of the silica under the gas phase reaction condition containing methanol [1]. Thus, the development of the non-noble metal and non-silica catalysts for the hydrogenation of DMO operating at high LHSV has increased tremendous interests in both academia and industry. Moreover, it is greatly significant and valuable for the achievement of the co-production of the MG and EG on only one catalyst in the same plant depending on the production requirement or the reaction condition.

In the present work, a novel kind of copper based HAP supported catalyst is systematically studied to investigate the relationship between the structure–function and the selective behavior of the catalysts. HAP is one of the calcium phosphate salts which are the mineral constituent of human hard tissues (bones, teeth, etc.) and are of importance in the biomedical field as a raw material for the preparation of artificial bone graft. It is also a promising material used industrially in sensors, fluorescence materials, chromatography, and environmental phosphorus recovery. As a catalyst, HAP has the unusual property of containing both acidic and basic sites in a single crystal lattice and exhibits superb catalytic performance in formaldehyde combustion [17], catalytic conversion of ethanol [18], and catalytic reduction of NO_x [19]. Furthermore, HAP can be served as a catalyst support thanks to its high specific areas and ion-exchange property [19,20]. The HAP carrier would also afford abundant hydroxyl groups and moderate acid property on the surface of the catalysts which would contribute to the hydrogenation of DMO to MG and EG [2]. The as-prepared Cu/HAP catalysts in the present work show higher selectivity to MG compared with other Cu based catalysts, moreover, the selectivity to EG could be modulated simply only by controlling the reaction temperatures.

2. Experimental

2.1. Catalyst preparation

All the reagents are purchased from Sinopharm Chemical Reagent Co., Ltd. without further purification, unless otherwise specified.

Copper based HAP catalysts are synthesized via a facile ammonia-assisted one-pot synthesis (AAOPS) method. Firstly, 7.56 g of $Ca(NO_3)_2{\cdot}4H_2O$ is dissolved in 300 ml of deionized water and a certain amount of aqueous ammonia (25 wt.%) are added into the above solution to adjust the pH value to 11.0. Then, 0.1 M of $(NH_4)_2HPO_4$ aqueous solution is dripped slowly into the above suspension with the molar ratio of Ca/P to 1.67. The as-prepared suspension is then kept at 313 K for 24 h under stirring. Secondly, certain amount of $Cu(NO_3)_2{\cdot}3H_2O$ is added into the above suspension, and aqueous ammonia (25 wt.%) solution is added again to maintain the pH value at 11.0. Afterwards, the as-obtained suspension is kept on stirring for 4 h, and then, the bath temperature is risen to 363 K and the mixture is kept on stirring until the pH value of the suspension reaches 6–7. Finally, the filter cake is filtrated and washed with deionized water for three times. The solid is dried at 373 K overnight, and then, calcinated from 573 to 973 K at a ramping rate of 2 K min^{-1}.

Pure HAP can be obtained following the same procedure as-mentioned above without the addition of $Cu(NO_3)_2{\cdot}3H_2O$ and the calcination temperature is 773 K.

The added amount of $Cu(NO_3)_2{\cdot}3H_2O$ are determined by the copper loading. In our study, Cu/HAP catalysts with copper loading from 5 to 30 wt.% are synthesized and calcinated at 773 K, the catalysts are labeled as *x*Cu/HAP, where *x* stands for copper loading. Furthermore, the 20Cu/HAP catalysts at different calcination temperatures are further studied to confirm the structural evolution and the distinct catalytic sites on the catalysts. These catalysts are labeled as 20Cu/HAP-*y*, where y denotes the calcination temperatures (K).

All the catalysts are reduced at 573 K for 4 h under the 5% H_2/Ar (V/V) atmosphere prior to the catalytic test.

2.2. Catalyst characterization

Specific surface areas of the samples are measured by nitrogen adsorption–desorption method at 77 K (Micromeritics Tristar ASAP 3000) using Brunauer–Emmett–Teller (BET) method. The pore size distributions are obtained from the desorption isotherm branch of the nitrogen isotherms using Barrett–Joyner–Halenda (BJH) method.

The wide-angle XRD patterns are collected on a Bruker D8 Advance X-ray diffractometer using nickel-filtered Cu Kα radiation (λ = 0.15406 nm) with a scanning angle (2θ) range of 20–90°, a scanning speed of 2° min^{-1}, and a voltage and current of 40 kV and 40 mA, respectively. The full width at half maximum (FWHM) of CuO (0 1 1) and Cu (1 1 1) reflection is measured for calculating crystallite sizes using the Scherrer equation.

The copper loadings are determined by the inductively coupled plasma (ICP) method using a Thermo Electron IRIS Intrepid II XSP spectrometer.

TEM micrographs are obtained on a JOEL JEM 2010 transmission electron microscope. Samples for electron microscopy observation are prepared by grinding and subsequent dispersing the powder in ethanol and applying a drop of very dilute suspension on carbon-coated grids.

TPR profiles are obtained on a Tianjin XQ TP5080 auto-adsorption apparatus. 25 mg of the catalyst is outgassed at 473 K

under Ar flow for 2 h. After cooling to room temperature under Ar flow, the in-line gas is switched to 5% H_2/Ar, and the sample is heated to 703 K at a ramping rate of 10 K min^{-1}. The H_2 consumption is monitored by a TCD detector. The copper dispersion and the specific surface area of metallic copper (S_{Cu}) of the catalysts are measured by dissociative N_2O adsorption [21]. The specific area of metallic copper is calculated from the amount of H_2 consumption with 1.46×10^{19} copper atoms per m^2 [22].

X-ray photoelectron spectroscopy (XPS) experiments are carried out with a Perkin–Elmer PHI 5000C ESCA system equipped with a hemispherical electron energy analyzer. The Mg Kα ($h\nu$ = 1253.6 eV) anode is operated at 14 kV and 20 mA. The spectra are recorded in the constant pass energy mode with a value of 46.95 eV, and all binding energies are calibrated using the carbonaceous C 1s line at 284.6 eV as reference. The experimental errors are within ±0.2 eV.

2.3. Catalytic activities

The catalytic activity test is conducted using a fixed-bed reactor. Typically, 0.9 g of catalyst (40–60 meshes) sample are packed into a stainless steel tubular reactor (i.d. = 5 mm) with the thermocouple inserted into the catalyst bed. Catalyst activation is performed at 573 K for 4 h with a ramping rate of 2 K min^{-1} from room temperature under the 5% H_2/Ar (V/V) atmosphere. After cooling to the reaction temperature, 10 wt.% DMO (purity > 99%) in methanol and pure H_2 is fed into the reactor at a H_2/DMO molar ratio of 150 and a system pressure of 2.5 MPa. The reaction temperatures are set at 483 K or 513 K and LHSV of DMO is set at the value ranging from 0.2 to 1.0 h^{-1}. For the TOF values calculation, the LHSV of DMO is set at 1.6 h^{-1} to control the initial conversion lower than 20%. The products are condensed, and analyzed on a gas chromatograph (Finnigan Trace GC ultra) fitted with an HP-5 capillary column and a flame ionization detector (FID). The identification of the products is performed by using a GC–MS spectrometer; chromatography is performed on a Thermo Focus DSQ gas chromatograph with a mass-selective detector with electron impact ionization. Analyses are separated using a VF-5MS capillary column of 30 m × 0.25 mm with a phase thickness of 0.25 μm from HP, which was inserted directly into the ion source of the MS system.

3. Results

3.1. Characterization of the xCu/HAP catalysts

The physicochemical parameters of the *x*Cu/HMS catalysts are listed in Table 1. It is found that pure HAP owns a BET specific surface area of 113 $m^2 g^{-1}$, and interestingly, catalysts loaded with copper species display larger specific surface areas. These observations are also evidenced by the Stošić's research that the BET specific surface area would increase after a second metal is introduced into the HAP [23]. The 5Cu/HAP sample shows the highest specific surface area of 153 $m^2 g^{-1}$ and the excessively higher copper loading would decrease the specific surface area. The partial ion-exchange of Cu^{2+} with Ca^{2+} in the catalysts would be responsible for the increase in the specific area. The high copper content in the catalysts usually causes the agglomeration of the particles which could probably block the porous structure of the HAP and lead to the decrease of the specific areas. Thus, the 30Cu/HAP exhibits the smallest S_{BET} value.

The N_2 adsorption–desorption isotherm and the pore size distribution curves of the *x*Cu/HAP catalysts are shown in Fig. 1A and B, the hysteresis loop shapes of the N_2 adsorption–desorption of the pure HAP and the *x*Cu/HAP catalysts are extremely similar, revealing that the loading of certain amount of the copper species has little negative effects on the structure of the pristine HAP. Moreover, the pore sizes of the catalysts calculated from the BJH desorption branch are listed in Table 1, and small increases of the pore size could be observed on the catalysts with higher copper contents. The pore size distribution curves could provide more information on the catalyst structures. Pure HAP sample displays only one pore distribution peak at about 19 nm (see Fig. 1B). However, after loaded with copper species, another shoulder peak could be observed at about 29 nm, indicating that the copper species do have some impacts on the catalyst structure. With more copper loaded on the catalysts, the pore size distribution peaks become broadening and the shoulder peaks grow sharper. The increased pore size distribution could stem from the excess amounts of copper particles in the Cu/HAP catalysts, which vary the porous structure. In addition, the variation of the pore size distributions is also evidenced in the CuZnAl catalysts with high copper content [24].

XRD patterns for the calcinated *x*Cu/HAP catalysts are shown in Fig. 2A and B. Clear diffraction peaks at 32° and 26° characterizing the HAP phase could be distinguished in the pure HAP sample and the *x*Cu/HAP catalysts [23]. The diffraction peaks at 35.5°, 38.5°, 48.7°, 58.3°, 61.5°, 66.2° and 68.1° corresponding to the crystal planes of monoclinic CuO phase (JCPDS 05-0661) can be identified easily especially for the samples with higher copper loading. No other diffraction peaks related to the copper species or phosphates can be detected by the XRD measurement, indicating that the copper species are successfully loaded on the HAP supports via the AAOPS method. The particle sizes of the CuO species based on the Scherrer equation are also listed in Table 1. The 5Cu/HAP and 10Cu/HAP show much broader CuO diffraction peaks compared with other catalysts, implying that HAP is a promising support for the copper dispersion. Also, the 30Cu/HAP displays sharp CuO diffraction peaks, suggesting that too much copper species in the catalysts could lead to the aggregation of the copper oxide. For the reduced samples, obvious diffraction peaks at 43.3°, 50.4°, and 74.1° (JCPDS 04-0836) from metallic copper species can be picked out as shown in Fig. 2B. Higher copper contents in the catalysts would induce increases of the copper particle size. However, it is worth mentioning that owning to the strong ion-exchange property of the HAP species, there are definitely some of the copper cations

Table 1
Physicochemical parameters and the catalytic performances of the *x*Cu/HAP catalysts.

Catalysts	S_{BET} ($m^2 g^{-1}$)	V_{pore} ($cm^3 g^{-1}$)	D_{pore} (nm)	d_{CuO} [a] (nm)	d_{Cu} [a] (nm)	d_{Cu} [b] (nm)	STY_{MG} [c] (h^{-1})	STY_{EG} [d] (h^{-1})	C_{DMO} [e] (%)	TOF[e] (g/g_{Cu}) h^{-1}
HAP	113	0.56	19.8	–	–		–	–	–	–
5Cu/HAP	153	0.85	18.4	3.4	n.d.	2.1	0.48	0.50	1.9	2.6
10Cu/HAP	136	0.81	20.9	4.2	3.5	3.7	0.47	0.61	6.1	6.8
20Cu/HAP	128	0.65	22.5	6.3	5.6	5.2	0.56	0.72	18.2	14.4
30Cu/HAP	121	0.63	23.4	7.8	12.2	11.1	0.46	0.70	7.8	9.2

[a] CuO and Cu crystallite size calculated by the Scherrer formula.
[b] Copper particle sizes estimated by the TEM results with 300 particles.
[c] Space time yield. Reaction condition: 2.5 MPa, H_2/DMO = 150 mol/mol, and LHSV of DMO 0.4 h^{-1}, T = 483 K.
[d] Space time yield. Reaction condition: 2.5 MPa, H_2/DMO = 150 mol/mol, and LHSV of DMO 0.4 h^{-1}, T = 513 K.
[e] Reaction condition: 2.5 MPa, H_2/DMO = 150 mol/mol, and LHSV of DMO 1.6 h^{-1}, T = 483 K.

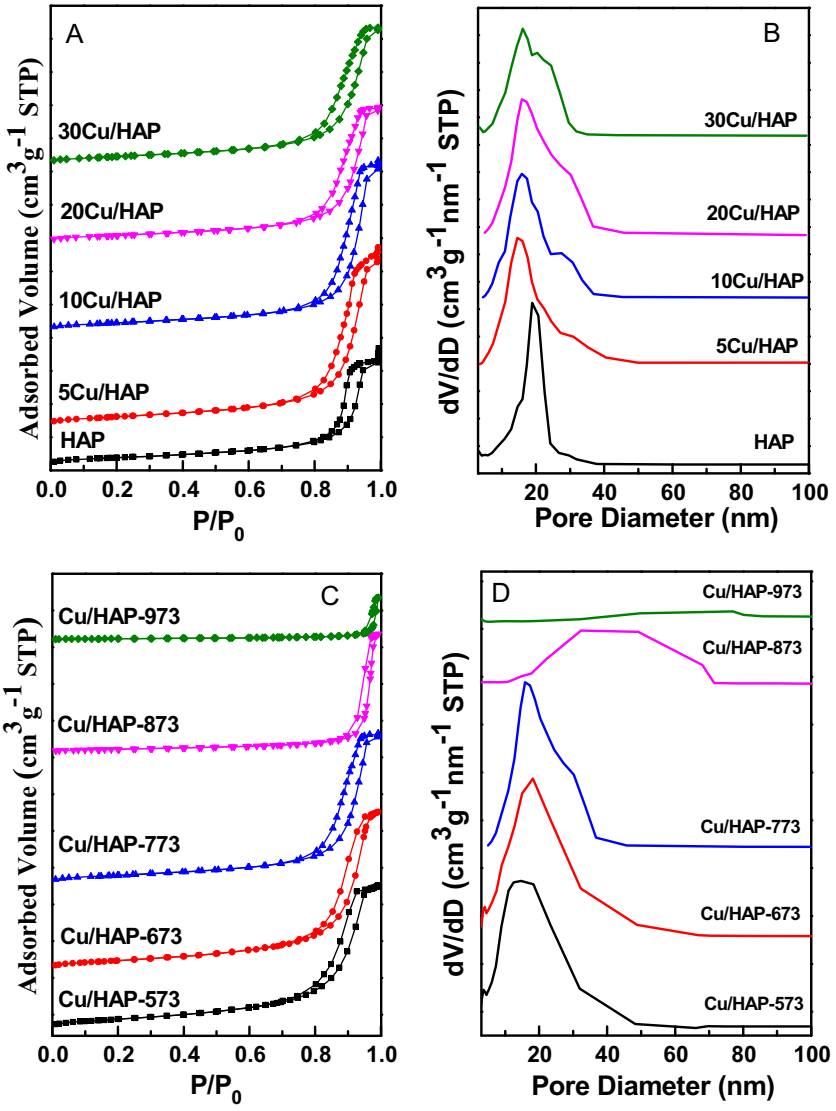

Fig. 1. N_2 adsorption–desorption isotherms of the *x*/HAP (A) and Cu/HAP-*y* catalysts (C); BJH pore size distribution of the *x*/HAP (B) and Cu/HAP-*y* catalysts (D).

embedded in the catalyst supports by the ion-exchanging between Cu^{2+} and Ca^{2+}; and furthermore, the synthesis of crystalline HAP requires high calcination temperature and other specific procedures which are quite different from the AAOPS method [25]. All of these reasons above can lead to the broadening of the diffraction peaks of the HAP species and the low crystalline degree of the catalysts.

TEM images for the reduced 20Cu/HAP sample are shown in Fig. 3. The catalyst particles are in flaky structure, which are similar to the pure HAP species (see Fig. S1), and the copper species are distributed homogeneously on the supports, indicating that pure HAP can be served as a proper carrier for the copper dispersion. The HRTEM image of the reduced catalyst illustrates the lattice fringes of 0.526 nm and 0.818 nm which fit well with the HAP (1 0 1) and HAP (1 0 0) planes respectively, confirming that the existence of the crystalline HAP structure. The lattice fringe of 0.208 nm corresponding to the metallic Cu (1 1 1) planes reveals that the successful synthesis of the HAP supported copper based catalysts. Furthermore, as shown in Fig. S1, the copper particles grow with the increase of the copper loading, and clear aggregation of the copper species could be observed in the 30Cu/HAP. The metal particle size distributions of the *x*Cu/HAP catalysts estimated from the TEM results of 300 particles are shown in Fig. S2. The average grain size of the copper particles is in well accord with the XRD results (see Table 1).

Reduction behavior of the *x*Cu/HAP catalysts is investigated by the TPR method and the results are shown in Fig. S3. There is no reduction peak for the pure HAP sample with temperature below 773 K. After loaded with the copper species, two obvious reduction peaks at 483 and 500–521 K could be observed which can be assigned to the well-dispersed copper species and the bulk copper species with large particle size. These findings accord well with other copper based catalysts, such as Cu/SiO_2 and CuZnAl catalysts [24,26]. However, there is a new reduction peak at about 560 K which can be attributed to the reduction of the copper phosphate species or other libethenite phase and other copper species with large particle size [19]. It should be noted that the reduction peak in the 5Cu/HAP is mainly at low temperature regions, suggesting that the copper species are mostly in well-dispersed state or easily reduced bulk state. With the copper loading increasing, the reduction peak at 620 K becomes obvious. The high reduction temperature peaks are ascribed to the reduction of the copper species embedded into the HAP frameworks or the copper phosphate species formed in the ion-exchange process. Moreover, the copper species with large particle size also could not be excluded. The 30Cu/HAP catalyst displays a large and broad

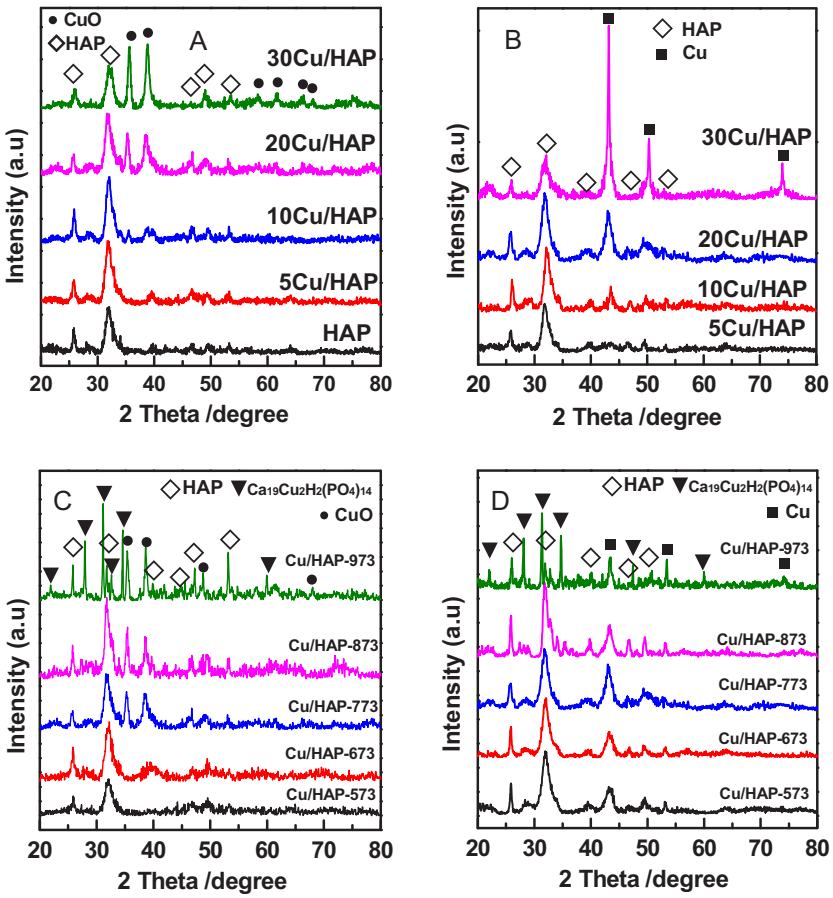

Fig. 2. XRD patterns of the catalysts. (A) *x*Cu/HAP calcinated at 773 K; (B) *x*Cu/HAP reduced at 553 K; (C) Cu/HAP-*y* after calcination; (D) Cu/HAP-*y* reduced at 573 K.

reduction peak at higher than 600 K due to its excess high copper content.

Generally, the phosphate groups in HAP would endow the certain amount of acidity for the catalyst and NH_3-TPD is carried out to evaluate the total acidity of the synthesized HAP supported catalysts. As shown in Fig. 4A, there are two desorption peaks for pure HAP and the supported catalysts. The desorption temperatures and the peak areas are calibrated to quantitatively study the acid contents and basically, the higher desorption temperature is, the stronger the acid strength is. The desorption peaks at about 500 K could be assigned to the weak acid sites for the HAP which is consistent with Ghantani's work [27]. Moreover, pure HAP also shows a desorption peak at about 620 K, indicating that there is a small amount of strong acid sites located on the HAP surface. Interestingly, after loaded with copper species the total amount of the acid sites is greatly increased and the results are listed in Table S1. It should be noted that the amounts of weak acid sites are first enhanced after loading with Cu species on the HAP with Cu content of 0.25 mmol/g and then decreased with the increase of copper loading. The enhanced acid amount can be attributed to the ion-exchange effect between Cu^{2+} and Ca^{2+} because the Ca^{2+} ions in the HAP structure are responsible for the basicity.

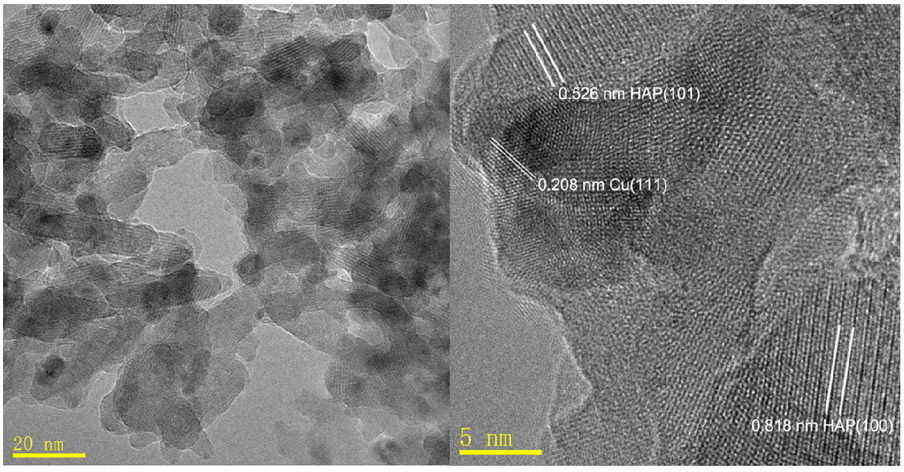

Fig. 3. TEM images of 20Cu/HAP.

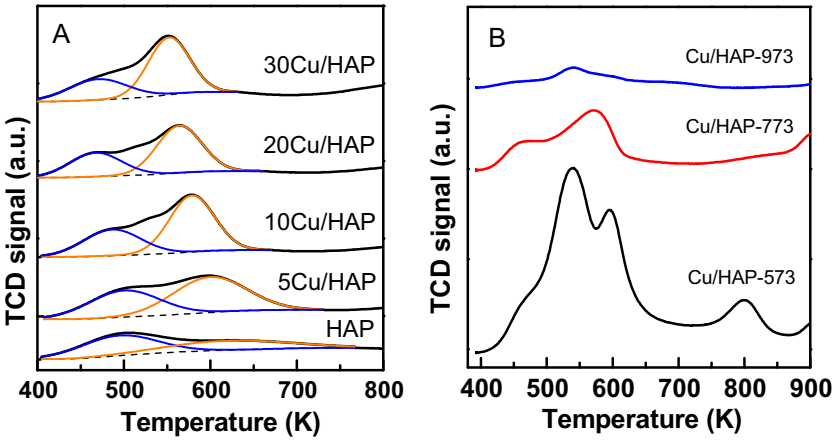

Fig. 4. NH_3-TPD profiles of the *x*Cu/HAP (A) and Cu/HAP-*y* catalysts (B).

Furthermore, the desorption peaks at 620 K, which stand for the stronger acid or moderate acid sites, seem constant for all the *x*Cu/HAP catalysts. The enhanced acid amount with a similar surface distribution content is resulted from the decomposition of the copper ammonia complex (NH_3 bonded at Cu cationic species) at around 600 K, and this finding is also observed in Putluru's work [28]. Thus, after loaded with copper species on the HAP support, the amounts of weak acid sites are obviously increased due to the ion-exchange between Ca^{2+} and Cu^{2+}.

The surface chemical states of the *x*Cu/HAP catalysts reduced at 773 K are carefully studied by XPS measurement. The XPS spectra of Cu 2p are shown in Fig. S4. The binding energies (BEs) of Cu $2p_{3/2}$ peak at 932.5 eV without the presence of the satellite peaks confirm that most of the surface copper species in the catalysts are in the reduced state. However, the discrimination of the Cu^0 and Cu^+ species from the Cu $2p_{3/2}$ spectra is quite difficult due to their overlapping BE values. The examination of the X-ray induced Auger spectra (XAES) Cu LMM could provide more accurate information to distinguish from the zero or mono valence states of copper. The curve-fitting of the Cu LMM XAES spectra and the deconvolution results are displayed in Fig. S4 and Table S1. The asymmetric Cu LMM peaks and the modified Auger parameter α' in the value of 1852 and 1848 eV definitely certify the co-existence of the Cu^0 and Cu^+ species on the surface of the catalysts. It should be pointed out that catalysts with higher copper loading would exhibit much amount of Cu^+ species which would be related to the poor reducibility of the catalysts. Surprisingly, both the broad Cu $2p_{3/2}$ peak and the presence of a protuberance at the peak position of 935.5 eV as shown in Fig. S4(B) reveal that tiny amount of Cu^{2+} species which can be the copper species embedded into the HAP supports definitely exist on the surface of the catalysts. Furthermore, the TPR results also confirm the incomplete reduction state of the copper species at the temperature below 573 K. The Cu^{2+} species derived from the copper phosphate species or other libethenite phases during the synthetic process could not be neglected and the relative ratio of the Cu^{2+} is listed in Table S1. Moreover, the presence of the embedded copper species into the HAP structure would play an important role in the broadening of diffraction peaks for the HAP phase and the enhancement of the specific surface areas of the catalysts. It is found that the amounts of surface Cu^{2+} species on the catalysts seem relatively constant with the variation of the copper loading compared with the changes of Cu^0 and Cu^+, suggesting that the formation of the embedded copper species or copper phosphate are saturated even though higher content of copper species are introduced. The excess higher copper amount in the catalyst would block the reduction of copper species to some extent and cause the decrease of the metallic copper species on the catalysts and the relatively high ratio of Cu^+/Cu^0 in the 20Cu/HAP and 30Cu/HAP.

Hydrogenation of DMO is carried out to testify the catalytic activity of the Cu/HAP catalysts. The tandem reaction, hydrogenation of DMO, would firstly produce the partial hydrogenation product MG, and further hydrogenation of MG would generate EG and EtOH, the latter of which would be predominant when the reaction temperature is risen to higher than 533 K [7]. It should be noted that previous studies on the Carberry number and the Wheeler–Weisz group on the hydrogenation process of DMO have shown that mass transfer limitations could be negligible [6,26].

The catalytic properties of the *x*Cu/HAP catalysts under 483 K and 513 K examined by the LHSV are displayed in Fig. 5. Pure HAP does not show any catalytic activity in the hydrogenation of DMO. The 20Cu/HAP catalyst exhibits the highest conversion compared with the other catalysts at 483 K, indicating its superb catalytic activity, and the 5Cu/HAP displays the poorest catalytic activity even at a relatively low LHSV of 0.2 h^{-1}. Thus it can be concluded that the copper species are the main catalytic sites for the hydrogenation process. Generally, the conversion of DMO decreases with the increasing of the LHSV value due to the fact that more amounts of the reactants were pumped into the reactor, and also, the selectivity to the partial hydrogenation product MG would be enhanced. Interestingly, the 20Cu/HAP shows a relatively stable performance in the LHSV range of 0.3–0.7 h^{-1} and the yield to MG can be constant at about 70% which is significantly higher than any other counterparts (see Fig. S5). Fig. 6 shows the variations of catalytic performance on the 20Cu/HAP catalyst under different reaction temperatures. The conversion of DMO relies greatly on the reaction temperature and increases rapidly with the enhancement of the reaction temperature. MG is the dominant product at lower temperature and the yield of MG decreased with the increase of the DMO conversion. Furthermore, EG becomes the main product at the temperature of 513 K with 100% conversion of DMO and 90% selectivity. Other side-products including EtOH, 1,2-propanediol (1,2-PDO), and 1,2-butanediol (1,2-BDP) are generated due to the dehydration process [29]. Enhancing the reaction temperature or lowering the LHSV would cause the increment of the side-reaction and lead to a complexity in the product distribution. The catalytic activities are investigated on the *x*Cu/HAP catalysts at 483 K and 513 K respectively and the results are displayed in Fig. S6. Clear superiority in the DMO conversion for the 20Cu/HAP catalyst can be observed at the temperature of 483 K and the 20Cu/HAP catalyst exhibits the highest MG yield of 70%. Although the selectivity on the other catalysts is still high, the DMO conversion is low and further resulting in poor yield to MG. At higher reaction temperature, the selectivity shifts

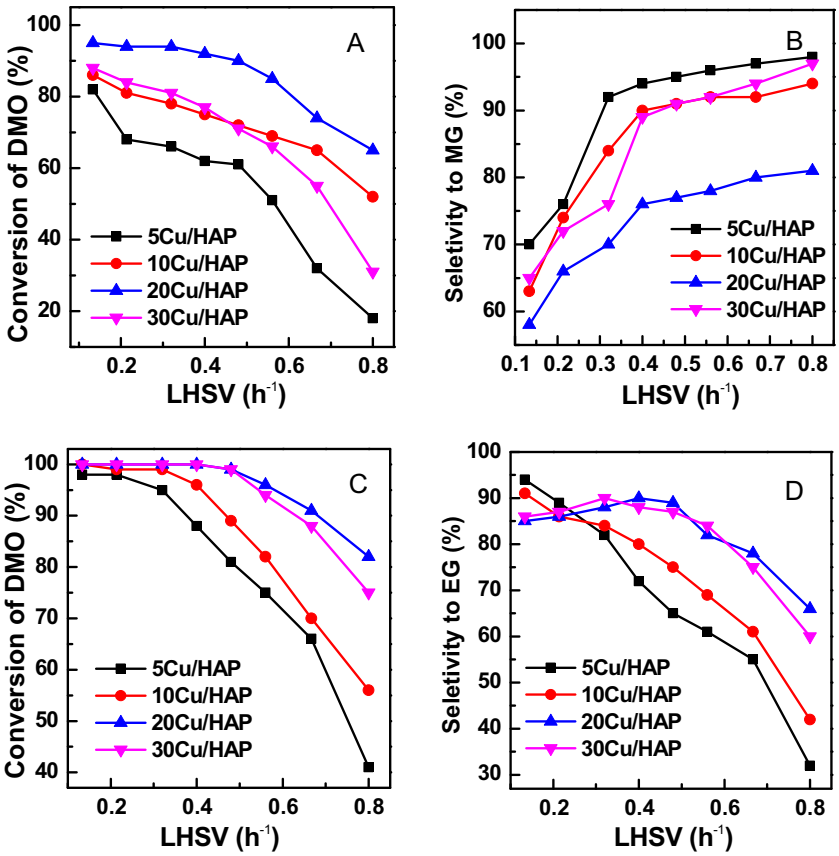

Fig. 5. Conversion of DMO on the *x*Cu/HAP catalysts under 483 K (A) and 513 K (C); selectivity to MG on the *x*Cu/HAP catalysts at 483 K (B); selectivity to EG on the *x*Cu/HAP catalysts at 513 K.

to EG and the differences on the catalytic behaviors of the catalysts become diminished and the 30Cu/HAP exhibits the activity on par with the 20Cu/HAP one, both the conversion and the selectivity are similar which can be interpreted as the saturated active sites on the catalysts with copper content higher than 20 wt.%. The space time yields (STY) on one gram of catalyst per hour are studied to evaluate the catalytic properties of the *x*Cu/HAP catalysts, and the 20Cu/HAP exhibits the highest STYs for MG at 483 K and 0.56 h^{-1} and EG at 513 K and 0.72 h^{-1} (see Table 1). Since the differences on the STYs of the *x*Cu/HAP catalysts seem minor, the TOF values of the catalysts are investigated to compare the catalytic activities of the catalyst based on the grams of DMO converted on per gram of surface sites per hour. The 20Cu/HAP catalysts exhibit the highest TOF value, which is about 7 times higher than that of 5Cu/HAP and 1.5 times higher than those of 10Cu/HAP and 30Cu/HAP.

The long-time catalytic performance is studied on the 20Cu/HAP catalyst under 483 K and 513 K respectively and the results are presented in Fig. 7. The overall conversion of DMO and the selectivity to MG can be stabilized at 85 and 75% at 483 K. The catalyst can also run stably at 513 K with a full conversion of DMO and selectivity to EG higher than 90% without any deactivation even after 120 h of time on stream. The Cu/HAP catalysts own a long-term

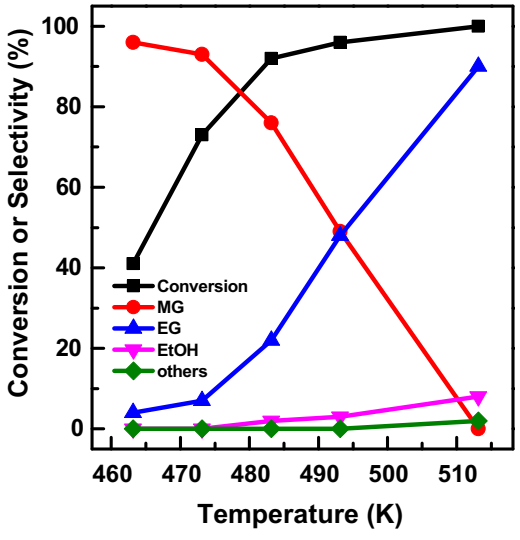

Fig. 6. Conversion and selectivity of the *x*Cu/HAP catalysts under different reaction temperatures.

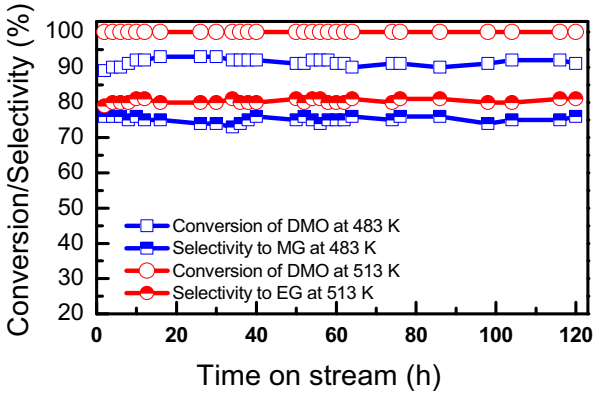

Fig. 7. Long time catalytic test on the 20Cu/HAP catalyst.

Table 2
Physicochemical parameters and the catalytic performance of the Cu/HAP-*y* catalysts.

Catalysts	S_{BET} ($m^2\ g^{-1}$)	V_{pore} ($cm^3\ g^{-1}$)	D_{pore} (nm)	d_{CuO} [a] (nm)	d_{Cu} [a] (nm)	d_{Cu} [b] (nm)	STY_{MG} [c] (h^{-1})	STY_{EG} [d] (h^{-1})	C_{DMO} [e] (%)	TOF[e] (h^{-1})
Cu/HAP-573	147	0.56	19.8	–	4.2	5.3	0.50	0.60	4	3.3
Cu/HAP-673	138	0.85	18.4	n.d.	4.5	4.8	0.54	0.70	11	8.1
Cu/HAP-773	128	0.65	21.4	6.3	5.6	5.2	0.56	0.72	18	14.4
Cu/HAP-873	48	0.65	22.5	7.2	5.7	7.9	0.53	0.66	12	14.6
Cu/HAP-973	17	0.63	23.4	10.6	10.4	15.5	0.46	0.34	2	5.3

[a] CuO and Cu crystallite size calculated by the Scherrer formula.
[b] Copper particle sizes estimated by the TEM results with 300 particles.
[c] Space time yield. Reaction condition: 2.5 MPa, H_2/DMO = 150 mol/mol, and LHSV of DMO 0.4 h^{-1}, T = 483 K.
[d] Space time yield. Reaction condition: 2.5 MPa, H_2/DMO = 150 mol/mol, and LHSV of DMO 0.4 h^{-1}, T = 513 K.
[e] Reaction condition: 2.5 MPa, H_2/DMO = 150 mol/mol, and LHSV of DMO 1.6 h^{-1}, T = 483 K.

catalytic lifespan and the catalytic active sites for EG and MG can remain unchanged during the long time catalytic test. Furthermore, the temperature-dependent measurements are also investigated. As shown in Fig. S7, the catalyst operated at 483 K for 5 h would obtain MG as the main product, then if raising the temperature to 513 K for another 5 h, the selectivity to EG increase gradually; further lowering the temperature to 483 K, MG would be the main products again. This finding implies the excellent thermal stability of the as-prepared Cu/HAP catalyst. The high catalytic performance of the Cu/HAP catalyst could be attributed to the moderate acid sites and the homogeneous dispersed copper species and also, small amount of copper phosphate species would play important roles in stabilizing the active copper species which would result in the long catalytic lifespan.

3.2. Characterization of the Cu/HAP-y catalysts

Generally, thermal treatment for the supported catalysts usually leads to the variation of the grain size, particle morphology, microstructures, phase composition, surface chemical properties and the acid–base properties [30]. To investigate the relationship between the catalytic properties and the catalyst structure, the 20Cu/HAP catalysts calcinated at different temperatures are carefully studied.

The physicochemical properties of the Cu/HAP-*y* catalysts are shown in Fig. 1C and Table 2. The observed hysteresis for a full range N_2 adsorption/desorption type IV isotherm with an increase in adsorption in the range of P/P_0 = 0.7–0.9 is due to the capillary condensation into the mesopores [31]. The hysteresis loop for the Cu/HAP-973 sample is unconspicuous, indicating the mesopore destruction happened during the calcination process. The BET specific surface areas of the catalysts decrease with the increasing of the calcination temperature, and the Cu/HAP-573 shows the highest S_{BET} value. The crystalline HAP species, which shows little porous structure, are more prominent under higher calcination temperature which would decrease the S_{BET} values of the catalysts [32]. The pore size distribution (PSD) of the catalysts is displayed in Fig. 1D. The PSD curves exhibit obvious right shift and widening with the increasing of the calcination temperature, confirming the destructive effect caused by the calcination process.

The calcination process plays a significant role in the crystallization of the catalysts and the physicochemical properties variations. The XRD patterns of the calcinated Cu/HAP-*y* catalysts are shown in Fig. 2C. Under lower calcination temperatures, only the broad diffraction peak attributed to the HAP species could be recognized. With the increasing of the calcination temperature, the diffraction peaks from CuO become obvious, more importantly, new peaks assigned to the $Ca_{19}Cu_2H_2(PO_4)_{14}$ phase (JCPDS 46-0412) can be observed clearly in the sample of Cu/HAP-973, suggesting the crystallization of the copper and the HAP species are enhanced and the phase transition between the metal and supports are definitely occurred during the calcination process under high temperature. It should be noted that the phase transitions of the calcium phosphate or other metal phosphates with the variation of the calcination temperatures are very common and widely reported [32]. XRD patterns for the catalysts reduced at 573 K show a tendency similar to that of calcinated catalysts. Catalysts calcinated at higher temperature would exhibit sharper diffraction peaks of metallic copper after reduction. Also, the $Ca_{19}Cu_2H_2(PO_4)_{14}$ phases can be observed (see Fig. 2D).

TEM images of the Cu/HAP-*y* catalysts are shown in Fig. S8. With the increase of the calcination temperatures, both the particles of copper and the HAP support exhibit noticeable changes. The copper particle size grows quickly when the catalyst was treated at the calcination temperature higher than 773 K. The morphologies of HAP supports are changed from the small sheet-like structure to large plate-like structure with the calcination temperatures increased from 573 to 973 K. The higher calcination temperature would induce the aggregation of the metal particle size and the phase transition of the HAP species. Furthermore, the generation of copper phosphates can be considered as the strong interaction between the copper species and the HAP supports.

The TPR measurement is also performed to investigate the reduction behavior of the series of Cu/HAP-*y* catalysts. As shown in Fig. S9, all the catalysts calcinated at temperatures from 573 to 773 K show three reduction peaks at temperatures of 510, 540 and 560 K. The two former reduction peaks should be the reduction of the well dispersed and bulk or crystalline copper species, and the peak at 560 K is attributed to the reduction of the copper phosphate species or other libethenite phase and other copper species with large particle size. It should be noted that for the catalysts calcinated at temperature higher than 773 K, the reduction peak at 510 K completely disappears, indicating that these catalysts consist of only bulk copper and the copper phosphate species. Furthermore, both the XRD measurement and the TEM images confirm the phase and morphology are changed under the different calcination process. Both the enlarged metallic copper particle size and the transformation from the small sheet-like to the plate-like structure of the HAP can be attributed to the effects caused by the calcination process.

The effect of calcination temperature on the surface acid–base properties is reported widely [32–34]. It is commonly accepted that the coverage by the carbonate species, the migration of other components from the bulk to the surface, the generation of new phases, and the variation of the functional groups all play very important roles in the surface acid–base properties. The Cu/HAP-573 exhibits the largest acid amount compared with Cu/HAP-773 and Cu/HAP-973 catalysts, and more importantly, there appears one desorption peak at 800 K, indicating that the acid strength of the Cu/HAP-573 is stronger than the other counterparts (see Fig. 4B). The Cu/HAP-773 shows the moderate acid amount and the Cu/HAP-973 exhibits little acid amount due to the extremely small NH_3 desorption peak. Catalysts calcinated at a lower temperature would generate more surface hydroxyl groups which would be beneficial for the acid

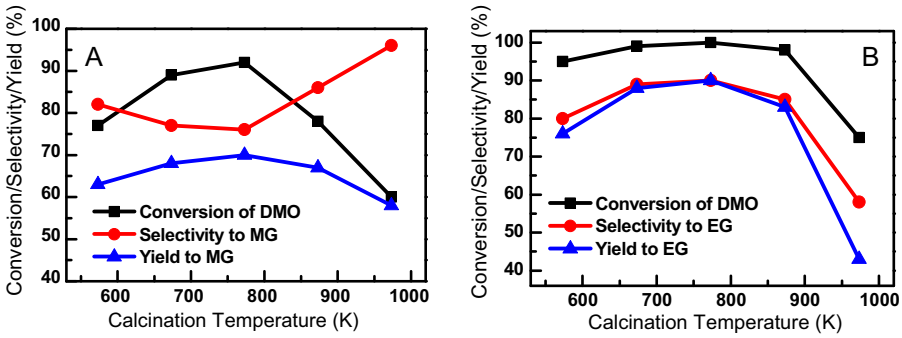

Fig. 8. Catalytic performances of the Cu/HAP-*y* catalysts. Reaction temperature at 483 K (A) and 513 K (B).

property. Conversely, the higher calcination temperature would decrease the amount of hydroxyl groups. In addition, the crystalline grain size would increase more easily during the higher temperature thermal treatment, and the higher calcinations temperature further results in the collapse of the porous structure and the coverage of acid sites [35]. Thus, the catalysts after higher temperature treatment exhibit low S_{BET} values, the poor reduction behavior, and the decrease of the acid amounts.

To further confirm the variation of the surface hydroxyl groups during the calcination process, the Fourier transform infrared (FT-IR) technique is applied to investigate the distinctive surface functional groups on the catalysts, and the results are shown in Fig. S10. The bands at 561, 598, 1039, 1090 cm^{-1} are assigned to the ν_4 and ν_3 bands of PO_4^{3-} modes respectively, which suggest that the HAP are successfully synthesized via the AAOPS method. Broad bands appearing at wave number value of 1420 and 1480 cm^{-1} are indicative of the carbonate ion due to carbonate incorporation process which is often observed in the literature for several HAP samples [36]. The band at around 3440 cm^{-1} due to the adsorbed water overlaps and the weak bands at around 3565 cm^{-1} (see the insert in Fig. S10), which is due to the structural OH, can be clearly observed [37]. Both peak intensities of the carbonate and hydroxyl groups show a decreasing trend with the increase of the calcination temperature. The carbonate species would decompose under higher calcination temperature and the hydroxyl groups, which were derived from the abundant P—OH groups on the HAP surface [38], are also affected by the elevated temperatures, suggesting the decreasing amount of the surface hydroxyl groups [36].

The catalytic behaviors of the Cu/HAP-*y* catalysts are compared and the results are displayed in Fig. 8. When the reaction temperature is set at 483 K with a LHSV of 0.4 h^{-1}, the main hydrogenation product is MG, and the conversions for the catalysts under different calcination temperatures exhibit a volcanic type curve and the Cu/HAP-773 gives the highest conversion (see Fig. 8A). However, the selectivity to MG presents an opposite tendency and the Cu/HAP-773 shows the lowest selectivity at 76%. Most importantly, although the Cu/HAP-773 exhibits a poorer selectivity compared with the other samples, the highest yield to MG and STY value are obtained on this catalyst (see Table 2). Furthermore, the catalyst operating with poor conversion is much easier to deactivate, thus, the Cu/HAP-773 has distinct advantages compared with other counterparts. Elevating the reaction temperature to 513 K would shift the selectivity to EG and the conversion of DMO could also be enhanced (see Fig. 8B). The catalytic performance of the catalysts calcinated at 673–873 K show little differences under the reaction temperature of 513 K mainly because of the extreme sensitivity of the catalysts on the reaction temperatures and thus, the architectural differences caused by the calcination temperatures are very slight. However, the evaluation of the TOF values (see Table 2) can provide more subtle information on the catalytic activities of the catalysts. The catalyst calcinated at 773 and 873 K shows quite higher TOF values than that of the other ones. Taken the poorer Cu dispersion of the Cu/HAP-873 catalysts into consideration, the slightly higher TOF values and poorer STY values for Cu/HAP-873 seem more reasonable. The catalyst calcinated at 573 and 973 K exhibits much poorer catalytic activities compared with other catalysts. The excessively high or low heat treatment temperatures would induce the poor catalytic performance, which can be attributed to the poorer reducibility, the collapse of the porous structure or the aggregation of the particle sizes and even the phase transition of the HAP support.

4. Discussions

The reaction pathway of DMO hydrogenation is well demonstrated by Gong's group [39]. MG is obtained in the first hydrogenation step. However, the thermodynamic equilibrium constant of the first hydrogenation step is 2 orders of magnitude lower than that of the subsequent hydrogenation step, thus, it is difficult to suppress the further hydrogenation of MG to other products.

The Cu/HAP catalyst exhibits a distinct performance compared with the conventional Cu/SiO_2 catalysts. The as-synthesized Cu/SiO_2 catalysts via the ammonia evaporation method reported by Chen et al. shows 100% selectivity to EG, furthermore, the catalytic activity is relatively low [26]. The catalytic performance would be enhanced when a second metal or metal oxide is introduced into the Cu/SiO_2 catalyst and the yield to EG can be increased greatly even under higher LHSVs or lower reaction temperatures [4,5,29,39,40]. Based on the systematic study on the Cu based catalysts, the balanced Cu^+/Cu^0 proportion is considered as the key factor for the polarization of C=O bond and the activation of H_2 [6,7,39]. It is also found that Ag surfaces, compared to Cu, generally lack affinity toward H_2 dissociation, could benefit to the selective hydrogenation of DMO to the corresponding alcohols [13–16,39]. In addition, there are few studies focused on the selective synthesis of MG via DMO hydrogenation. In the present work, the 20Cu/HAP catalyst displays high selectivity to MG with the DMO conversion of 90% at 483 K, and most importantly, the catalysts can run stably for at least 120 h on the stream without any loss of catalytic activity (see Fig. 7). To the best our knowledge, this is the highest MG yield obtained from the hydrogenation of DMO over the copper based unitary catalysts. Furthermore, catalytic performance of the Cu/HAP catalyst synthesized by the AAOPS method is also comparable to the undecorated Cu/SiO_2 catalysts in the hydrogenation of DMO to EG, and the catalytic properties of the catalysts would be significantly enhanced by the further modifications. As we know, it would be practical and economical for industrialization of DMO hydrogenation with the only variation of the reaction temperatures. MG could be obtained under low temperatures and EG would be generated when the temperature is risen to 513 K. The long catalyst lifespan for the Cu/HAP catalysts also indicates the promising and encouraging prospect in

the industrialization of the hydrogenation process of DMO to MG and EG.

The catalytic performances of the *x*Cu/HAP catalysts are evaluated by the TOFs to probe the initial catalytic activities of the catalysts. The TOF values of the catalysts increase with the enhancement of the copper loading at first and the 20Cu/HAP shows the highest TOF value of 14.4 h^{-1} (see Table 1), implying that the copper species should be the main catalytic active sites. Moreover, the TOF values decrease when the excess amount of copper species are loaded on the HAP supports, suggesting the poor catalytic properties caused by the aggregation of the copper species. Although the STY values of the Cu/HAP-y catalysts seem similar, the TOFs of the catalysts display obvious differences and the superiority of the Cu/HAP-773 catalyst can be observed.

When the reaction temperature is set at 483 K, the main product on the Cu/HAP catalysts is MG. It is found that there are more Cu^+ species on the surface of the catalysts. The balance between the Cu^+ and Cu^0 is considered as the crucial factor for the DMO hydrogenation and the cuprous species could function as electrophilic or Lewis acidic sites to polarize the C=O bond via the electron lone pair in oxygen, thus improving the reactivity of the ester group in DMO [7]. In addition, our group also found that the Cu/SiO_2 catalysts decorated with metallic cobalt species display much higher catalytic activity in the generation of EG compared with the bare Cu/SiO_2 catalysts [5]. The enhanced catalytic properties can be attributed to the superb H_2 activation ability caused by the metallic cobalt species. From this point of view, to decrease the H_2 activation moderately would possibly avoid the generation of the deep hydrogenation product of EG and may have some positive effects for the MG synthesis. Fridman et al. studied the pathways of the cyclohexanol dehydrogenation reaction to cyclohexanone on copper-active sites with oxidation states of Cu^0 and Cu^+, and their results indicated that the dissociative adsorption of cyclohexanol on Cu^0 sites are accompanied by formation of cyclohexanol alcoholate species and phenolate species which would lower the selectivity of catalysts on this active site. However, the reactant absorbed on the Cu^+ species do not involve in the dissociative process [41]. Thus, it can be speculated that the Cu^+ species are more inclined to stabilize the intermediate product compared with the Cu^0 species. Although the H_2 activation procedure is important and indispensable in the hydrogenation of DMO process, too much of active hydrogen would further facilitate the deep hydrogenation product (EG). In the Cu/HAP catalysts, the copper phosphate with poor reducing capacity would lower the Cu^0 content and generate more amounts of active Cu^+ species during the reduction process just like the copper phyllosilicate in the Cu/SiO_2 catalysts [3] and facilitate the catalytic reaction to terminate in the MG step.

Certain amounts of Cu^{2+} species, which seem to have negative effects on the DMO hydrogenation process, are also detected. However, the existence of the Cu^{2+} species is indispensable for the metal-support interaction strengthening. It has been well established that the Ca^{2+} sites of HAP can be replaced by divalent cations such as Sr^{2+}, Ba^{2+}, Pb^{2+}, and Cu^{2+} [42], and both the TPR measurements and XPS results show the uncomplete reduction for the copper species under 573 K, indicating that the existence of Cu^{2+} species. The embedded copper species into the HAP lattice are hard to be reduced and could help to increase the specific surface areas, to enhance the copper dispersions, and to generate more cuprous species during the reduction process [19]. The enlarged specific surface areas would enhance the reactant absorption and copper dispersion which further increase the catalytic activity. Moreover, the Cu^{2+} species would stabilize the Cu^+ species and improve the active specific surface areas.

The surface acid–base properties are equally important factors for the hydrogenation of DMO [29,43]. Generally, hydrogen-transfer reactions occur on acid sites, while hydrogenation reactions are greatly accelerated by the presence of a metal [44]. Although the Cu/HAP-573 exhibiting the small copper particle and the higher S_{BET} value, which seem to contain all the elements for a highly efficient catalyst, the Cu/HAP-773 with moderate content of acid sites shows the highest yield to MG. Generally, strong acid sites would induce the intermolecular reactions and decrease the catalytic activity of the Cu based catalysts [26]. Taken the discussion into consideration, the poor catalytic performance of the Cu/HAP-573 seems much more acceptable. Thus, the moderate acid content should be another factor for the high selectivity for the Cu/HAP catalyst.

Beyond the strong interaction of the Cu and the HAP species and the moderate acid property of the HAP supports, another structural feature of HAP is the abundant amounts of surface hydroxyl groups, which would play important roles in the catalytic hydrogenation process. Qu et al. [45] reported an interesting finding that the catalytic performance of supported Ag/SiO_2 catalysts toward the selective oxidation of CO in the presence of excess amount of hydrogen at low temperature could be greatly enhanced by pretreating the SiO_2 support before catalyst preparation. They thought that calcination of SiO_2 at appropriate temperature preferentially removed the H-bonded SiOH, which resulted in the highly dispersive Ag/SiO_2 catalyst and thus improved the catalytic performance. In the present work, as the increase of the treatment temperature from 573 to 973 K, the surface hydroxyl groups decrease obviously, and the decrease of the yield to MG is also observed. This finding, consistent with Yin's study [13], strongly suggests that the hydroxyl groups on the surface of the catalysts could facilitate the hydrogenation of DMO to MG. Furthermore, enhanced amount of hydroxyl groups can also increase the weak acid amount of the catalysts [46] and seem to be much easier for the MG desorption compared with the EG species [47]. The yield to MG on the Cu/HAP catalysts is lower compared with the Ag or Au based catalyst, and the inert H_2 dissociation ability on the Ag^0/Ag^+ and Au^0 compared to the Cu^0 would greatly facilitate the MG selectivity. For the Cu/HAP catalysts, the high H_2 activation capacities of the Cu^0 species are relatively reduced at 483 K which results in the catalytic reaction terminating on the first hydrogenation product of MG. Furthermore, the surface properties of the HAP supports are also beneficial to the MG synthesis due to the abundant hydroxyl groups and the acid sites which can work as the Cu^+ species to stabilize the C=O groups. Both the above-mentioned effects make the Cu/HAP a promising catalyst in the selective hydrogenation of DMO to MG.

When the reaction temperatures are risen up to 513 K, the catalytic products shifted to EG. The hydrogenation of DMO is highly sensitive to the catalytic reaction temperature which are discussed widely [2,3,7,15], and higher reaction temperature would facilitate the generation of the deep hydrogenation products. The Cu/SiO_2 catalysts display superb catalytic activity and the EG would be the main product under the reaction temperature at 463–513 K. Moreover, EtOH would be generated under the reaction temperature at 533–573 K. Hydrogenation of DMO to EG at 513 K over the Cu/HAP catalysts can be also achieved and the catalytic performance is comparable to the pure Cu/SiO_2 catalysts [26]. It can be presumed that the Cu/HAP retains its hydrogenation activity with only weakening its H_2 activation capacity at lower reaction temperature. Both the abundant hydroxyl groups and the weakened hydrogen activation ability facilitate the high selectivity to the MG product with long catalytic lifespan. If the reaction temperatures are set at 513 K, the hydrogen activation process of the Cu/HAP catalyst is enhanced and the catalytic products of EG become the main product and the catalytic behavior of the Cu/HAP is just like the conventional Cu/SiO_2 catalysts. This finding is very promising and encouraging and would make a great contribution to the hydrogenation process

of DMO, considering the super stability of HAP under the reaction conditions if compared with SiO_2 support.

5. Conclusions

The Cu/HAP catalysts are synthesized by the AAOPS method and are applied in the reaction temperature controlled selective hydrogenation of DMO to MG and EG. The results show that MG is the main product of the reaction at low reaction temperature over the Cu/HAP catalysts. The relatively low hydrogen activation ability and abundant hydroxyl groups can facilitate the high selectivity to MG. The catalytic behavior for the Cu/HAP catalysts at high reaction temperatures is similar to the conventional Cu/SiO_2 catalysts, generating EG as the main product. The Cu/HAP catalysts are very stable even after 120 h of running without any loss of catalytic activities both at 483 and 513 K. The AAOPS synthetic method would provide an innovative way for the nanocomposites synthesis and the as-synthesized Cu/HAP catalysts can definitely contribute to the industrialization of the hydrogenation of DMO or other catalytic reactions in the clean utilization of coal resource.

Acknowledgements

We would like to thank financial support by the Major State Basic Research Development Program (Grant No. 2012CB224804), NSFC (Project 21373054, 21173052), State Key Laboratory of Catalytic Materials and Reaction Engineering (RIPP, SINOPEC) and the Natural Science Foundation of Shanghai Science and Technology Committee (08DZ2270500). We also thank Dr. Songhai Xie for the TEM experiments.

Appendix A. Supplementary data

Supplementary material related to this article can be found, in the online version, at http://dx.doi.org/10.1016/j.apcatb.2014.07.023.

References

[1] C. Wen, Y. Cui, W.L. Dai, S. Xie, K.N. Fan, Chem. Commun. 49 (2013) 5195.
[2] A. Yin, C. Wen, W.L. Dai, K.N. Fan, Appl. Catal. B: Environ. 108–109 (2011) 90.
[3] H. Yue, Y. Zhao, S. Zhao, B. Wang, X. Ma, J. Gong, Nat. Commun. 4 (2013) 2339.
[4] C. Wen, A. Yin, Y. Cui, X. Yang, W.L. Dai, K.N. Fan, Appl. Catal. A: Gen. 458 (2013) 82.
[5] C. Wen, Y. Cui, W.L. Dai, K.N. Fan, ChemCatChem 5 (2013) 138.
[6] S. Zhao, H. Yue, Y. Zhao, B. Wang, Y. Geng, J. Lv, S. Wang, J. Gong, X. Ma, J. Catal. 297 (2013) 142.
[7] J. Gong, H. Yue, Y. Zhao, S. Zhao, L. Zhao, J. Lv, S. Wang, X. Ma, J. Am. Chem. Soc. 134 (2012) 13922.
[8] J.S. Lee, J.C. Kim, Y.G. Kim, Appl. Catal. 57 (1990) 1.
[9] S.A.I. Barri, D. Chadwick, Catal. Lett. 141 (2011) 749.
[10] D.J. Loder (1939). US Patent 2, 152, 852.
[11] U. Matteoli, G. Menchi, M. Bianchi, F. Piacenti, J. Mol. Catal. 44 (1988) 347.
[12] U. Matteoli, J. Organomet. Chem. 22 (1984) 353.
[13] A. Yin, X. Guo, W. Dai, K. Fan, Chem. Commun. 46 (2010) 4348.
[14] J. Zheng, H. Lin, X. Zheng, X. Duan, Y. Yuan, Catal. Commun. 40 (2013) 129.
[15] J. Zheng, H. Lin, X. Zheng, X. Duan, Y. Yuan, J. Catal. 297 (2013) 110.
[16] B. Wang, Q. Xu, H. Song, J. Xu, J. Nat. Gas Chem. 16 (2007) 78.
[17] J. Xu, T. White, P. Li, C. He, Y. Han, J. Am. Chem. Soc. 132 (2010) 13172.
[18] T. Tsuchida, J. Kubo, T. Yoshioka, S. Sakuma, T. Takeguchi, W. Ueda, J. Catal. 259 (2008) 183.
[19] H. Tounsi, S. Djemal, C. Petitto, G. Delahay, Appl. Catal. B: Environ. 107 (2011) 158.
[20] H. Sun, F.Z. Su, J. Ni, Y. Cao, H.Y. He, K.N. Fan, Angew. Chem. Int. Ed. 48 (2009) 4390.
[21] Z.Y. Pu, X.S. Liu, A.P. Jia, Y.L. Xie, J.Q. Lu, M.F. Luo, J. Phys. Chem. C 122 (2008) 15045.
[22] C. Chinchen, C.M. Hay, H.D. Vandervell, K.C. Waugh, J. Catal. 103 (1987) 79.
[23] D. Stošić, S. Bennici, S. Sirotin, C. Calais, Appl. Catal. A: Gen. 447–447 (2012) 124.
[24] C. Wen, F. Li, Y. Cui, W.L. Dai, K.N. Fan, Catal. Today 233 (2014) 117–126.
[25] T.A. Kuriakose, S.N. Kalkura, M. Palanichamy, D. Arivuoli, K. Dierks, G. Bocellif, C. Betzel, J. Cryst. Growth 1–4 (2004) 517.
[26] L.F. Chen, P.J. Guo, M.H. Qiao, S.R. Yan, H.X. Li, W. Shen, H.L. Xu, K.N. Fan, J. Catal. 257 (2008) 172.
[27] V.C. Ghantani, S.T. Lomate, M.K. Dongare, S.I.B. Umbarkar, Green Chem. 15 (2013) 1121.
[28] S.S.R. Putluru, A. Riisager, R. Fehrmann, Appl. Catal. B: Environ. 101 (2011) 183.
[29] Z. He, H. Lin, P. He, Y. Yuan, J. Catal. 277 (2011) 54.
[30] D.E. Lopez, K. Suwannakarn, D.A. Bruce, J.G. Goodwin Jr., J. Catal. 247 (2007) 43.
[31] H.S. Cho, R. Ryoo, Micropor. Mesopor. Mater. 151 (2012) 107.
[32] D. Bernache-Assollant, A. Ababou, E. Champion, M. Heughebaert, J. Eur. Ceram. Soc. 23 (2003) 229.
[33] S. Casenave, H. Martinez, C. Guimon, A. Auroux, Thermochim. Acta 379 (2011) 85.
[34] J.R. Sohn, S.H. Lee, J.S. Lim, Catal. Today 116 (2006) 143.
[35] C. Sun, J.C. Berg, Adv. Colloid. Interface 105 (2003) 151.
[36] R.N. Panda, M.F. Hsieh, R.J. Chung, T.S. Chin, J. Phys. Chem. Solids 105 (2003) 151.
[37] S. Koutsopoulos, J. Biomed. Mater. Res. A 62 (2002) 600.
[38] H.W. Choi, H.J. Lee, K.J. Kim, H.M. Kim, S.C. Lee, J. Colloid Interf. Sci. 304 (2006) 277.
[39] H. Yue, X. Ma, J. Gong, Acc. Chem. Res. 47 (2014) 1483.
[40] X. Zheng, H. Lin, J. Zheng, X. Duan, Y. Yuan, ACS Catal. 12 (2013) 2738.
[41] V.Z. Fridman, A.A. Davydov, K. Titievsky, J. Catal. 222 (2004) 545.
[42] B.M. Choudary, C. Sridhar, M.L. Kantam, B. Sreedhar, Tetrahedron Lett. 45 (2004) 7319.
[43] H. Lin, X. Zheng, Z. He, J. Zheng, X. Duan, Appl. Catal. A: Gen. 445–446 (2012) 287.
[44] G.W. Huber, A. Corma, Angew. Chem. Int. Ed. 46 (2007) 7184.
[45] Z.P. Qu, W.X. Huang, M.J. Cheng, X.H. Bao, J. Phys. Chem. B 109 (2005) 15842.
[46] A. Jentys, K. Kleestorfer, H. Vinek, Micropor. Mesopor. Mater. 27 (1999) 231.
[47] S. Kwon, R. Vidic, E. Borguet, Surf. Sci. 522 (2003) 17.